# CORTICOMOTONEURONAL MODEL FOR INTRAOPERATIVE NEUROPHYSIOLOGICAL MONITORING DURING DIRECT BRAIN STIMULATION

**JOSE GOMEZ-TAMES[*] and AKIMASA HIRATA[†]**

*Department of Electromechanical Engineering, Nagoya Institute of Technology*
*Nagoya, Aichi 466-8555, Japan*
[*]*jgomez@nitech.ac.jp*
[†]*ahirata@nitech.ac.jp*

**MANABU TAMURA[‡] and YOSHIHIRO MURAGAKI[§]**

[‡§]*Faculty of Advanced Techno-Surgery, Institute of Advanced Biomedical Engineering and Science, Tokyo Women's Medical University*
*Shinjuku-ku, Tokyo 162-8666, Japan*
[‡§]*Department of Neurosurgery, Neurological Institute, Tokyo Women's Medical University*
*Shinjuku-ku, Tokyo 162-8666, Japan*
[‡]*tamura.manabu@twmu.ac.jp*
[§]*ymuragaki@abmes.twmu.ac.jp*

Intraoperative neurophysiological monitoring during brain surgery uses direct cortical stimulation to map the motor cortex by recording muscle activity induced by the excitation of alpha motor neurons (MNs). Computational models have been used to understand local brain stimulation. However, no a computational model revealing the stimulation process from the cortex to MNs has not yet been proposed. Thus, the aim of the current study was to develop a corticomotoneuronal (CMN) model to investigate intraoperative stimulation during surgery. The CMN combined the following three processes into one system for the first time: 1) induction of an electric field in the brain based on a volume conductor model; 2) activation of pyramidal neurons with a compartment model; and 3) formation of presynaptic connections of the pyramidal neurons to MNs using a conductance-based synaptic model coupled with a spiking model. The implemented volume conductor model coupled with the axon model agreed with experimental strength-duration curves. Additionally, temporal/spatial and facilitation effects of corticomotoneuronal synapses were implemented and verified. Finally, the integrated CMN model was verified with experimental data. The results demonstrated that our model was necessary to describe the interaction between frequency and pulses to assess the difference between low-frequency and multi-pulse high-frequency stimulation in cortical stimulation. The proposed model can be used to investigate the effect of stimulation parameters on the cortex to optimize intraoperative monitoring.

*Keywords*: Direct cortical stimulation; corticomotoneuronal model; intraoperative neurophysiological monitoring; excitatory post-synaptic potential; neurosurgery

---

[*] Corresponding Author

## 1. Introduction

Intraoperative mapping and monitoring is an electrophysiological technique, where direct cortical and subcortical stimulation is applied to identify and monitor structures of the primary motor cortex and pyramidal tract. This prevents neurological deterioration during brain tumor surgery, while maximizing resection to increase the survival rate.[1–3] The risk of motor dysfunction is reduced by detecting the following: a reduction or alteration of the motor evoked potentials (MEPs) in the muscles of the upper and lower limbs,[4] descending motor volleys (D-wave) from the epidural space in the spinal cord,[5] or voluntary movements during awake craniotomy.

The induced electric field modulates neuronal activity in the cortical and subcortical structures by depolarization or hyperpolarization of nervous tissue. The degree of excitation or inhibition is determined using the electric field distribution and electrophysiological properties of the neuron. The electric field distribution is affected by anatomical geometry,[6–8] electrical conductivity of the tissues,[9–12] and stimulation parameters.[13]

During intraoperative mapping and monitoring, a variety of parameters, such as the type of pulse (monophasic or biphasic and cathodal or anodal), stimulation probe (monopolar or bipolar), pulse duration, frequency, and intensity are available.[1] In the cortex, anodal stimulation activates neuronal cells with lower intensity than cathodal stimulation because of the roughly perpendicular orientation of nerves along the electric field.[14] In contrast, cathodal stimulation is preferential for the subcortical region, as descending neurons are approximately parallel to the electrodes.[15] Stimulation is delivered using low frequency (LF) at 50 Hz[16] or high frequency (250–500 Hz) at different pulse duration (i.e., 0.1–0.7 ms; 3–10 pulses).[17] High-frequency multi-pulse train (HF) stimulation is used to enhance the response by a temporal facilitation process at the synaptic level in lower motor neurons (MNs). The activation threshold is also reduced for longer pulse durations as described by the strength-duration curve. A complete review of commonly employed parameters in clinical intraoperative mapping and monitoring can be found in Saito et al (2015).[1]

During cortical stimulation, descending action potentials travel through the corticospinal axons, which synapse with the anterior horn, where cell bodies of alpha MNs are located. An excitatory postsynaptic potential (EPSP) is generated in the postsynaptic membrane, which can elicit an action potential that travels to the endplate, producing an MEP. Thus, in addition to acting on the number of activated pyramidal neurons at the cortical level, stimulation conditions/parameters also have an effect at the synaptic level, where MN responses are enhanced by temporal/spatial summation and neural facilitation. A computational model that predicts the effect of different stimulation scenarios using integration of cortical stimulation and synaptic effects is warranted to improve intraoperative neurophysiological mapping and monitoring by visualizing activated area and finding optimal stimulation parameters.

From a physics viewpoint, several computational studies have estimated the effect of stimulation parameters on the electric field distribution in nervous tissue.[18–22] Stimulation parameters have also been investigated for epidural and subdural stimulation,[14,23,24] by combining volume conductor and compartment neuron models. In the case of intraoperative mapping and monitoring, in particular, only one study[25] has investigated the effects of cerebrospinal fluid (CSF) on the electric field distribution during transcranial electrical stimulation. These volume conductor models for brain stimulation focused on the local activation of the brain, without combining other neuronal systems (e.g., synaptic effects[26–29]). If these systems can be integrated, the resulting electrophysiological response from electrostimulation of the motor cortex can be estimated.

The current study proposes a new corticomotoneuronal (CMN) model to describe the activation process from cortical stimulation to MEP, by computing the following three steps: the induced electric field in the brain based on a volume conductor model, activation of pyramidal cells with the compartment axon model, and presynaptic connections to a MN using a conductance-based synaptic model coupled with a spiking model.

*Glossary*

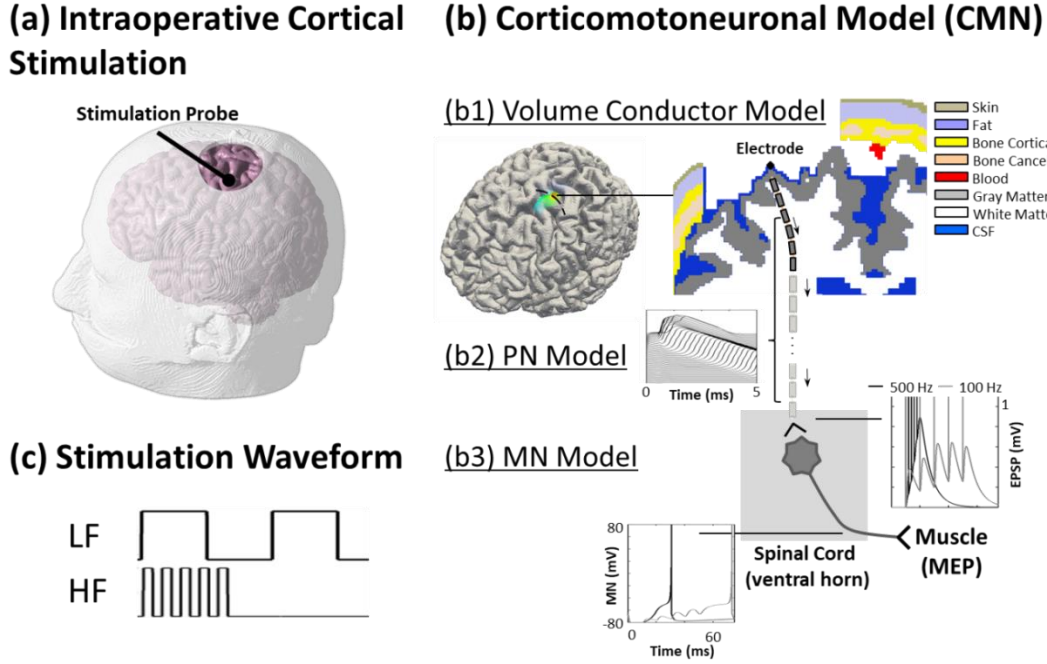| | |
|---|---|
| CMN | corticomotoneuronal |
| CRRSS | Chiu–Ritchie–Rogart–Stagg–Sweeney |
| EPSC | excitatory postsynaptic current |
| EPSP | excitatory postsynaptic potential |

Fig. 1. (a) Realistic head model with craniotomy similar to intraoperative cortical stimulation. (b) Proposed corticomotoneuronal (CMN) model for cortical stimulation is as follows: (b1) An externally applied field activates (b2) fast-conducting thickly-myelinated pyramidal neurons (PN) from the motor cortex. (b3) Some of these cortical motor fibers descend to and synapse directly on lower motor neurons (MNs), which extend to the motor end plates of the muscle. (EPSP: excitatory postsynaptic potential; MEP: motor evoked potential). (c) Illustration of the cortical stimulation waveforms: low-frequency (LF) and high-frequency multi-pulse train (HF) used in this study.

| | |
|---|---|
| HF | high-frequency multi-pulse train stimulation |
| LF | low-frequency stimulation |
| MEP | motor evoked potentials |
| MN | motor neuron |
| MRG | McIntyre-Richardson-Grill |

## 2. Method and Model

A three-step computational model of direct CMN stimulation was designed to explain the effect of externally applied electric fields on the temporal-spatial activation of target neurons, leading to motor evoked potentials (Fig. 1). In the first step, the electric potential generated by direct cortical stimulation was computed using a volume conductor model. In the second step, the induced electric potential obtained by the volume conductor model was coupled with a compartment model of a myelinated pyramidal neuron axon. Finally, the descending action potential through the corticospinal tract depolarizes the postsynaptic MN, which was implemented using a synaptic conductance model. The details of the implementation process are described in the following subsections.

### 2.1. *Volume Conductor Model*

The electric potential generated by the electrodes attached to the cortex was computed using the scalar potential finite difference method[30] to solve the following scalar potential equation:

$$\nabla(\sigma \nabla V_e) = 0, \qquad (1)$$

where $V_e$ and $\sigma$ denote the scalar potential and tissue conductivity, respectively. The potential[6] was solved iteratively using the successive-over-relaxation method and multigrid method.[31] The realistic head model was constructed from T1- and T2-weighted images (available on: http://hdl.handle.net/1926/1687) and represented by a grid of cubical voxels with a resolution of 0.5 mm.

The head model consisted of 14 tissues/body fluids (i.e., skin, fat, muscle, outer skull, inner skull, grey matter, white matter, cerebellar grey matter, cerebellar

white matter, brainstem, nuclei, ventricles, cerebrospinal fluid, and eyes,[6] some of which are shown in Fig. 1), and their conductive properties were modelled using the fourth order Cole-Cole model[32] at 10 kHz.

## 2.2. *Corticospinal Model*

The effects of the extracellular electric field on nerve activation are described by a compartment model of the neuron as introduced by McNeal.[33] The membrane potential $V_n = V_i$-$V_e$ for each compartment $n$ can be calculated as follows:

$$c_m \frac{dV_n}{dt} = -I_{ion,n} + 2 \left( \begin{array}{c} \frac{V_{n-1}-V_n}{R_{n-1}+R_n} + \frac{V_{n+1}-V_n}{R_{n+1}+R_n} \\ + \frac{V_{e,n-1}-V_{e,n}}{R_{n-1}+R_n} + \frac{V_{e,n+1}-V_{e,n}}{R_{n+1}+R_n} \end{array} \right), \quad (2)$$

where $c_m$ is the membrane capacitance, $I_{ion,n}$ the ionic current, $R$ the intra-axonal resistance between the centre of two adjacent compartments, and $V_e$ the extracellular potential, which allows the coupling with the volume conductor model described in section 2.1. The axon of a myelinated neuron consists of internodes (segments ensheathed by myelin) and nodes of Ranvier (ionic channels). The ionic membrane current through the myelinated internodes can be modelled by the passive conductance of the membrane, $G_{m,n}$, multiplied by the membrane potential ($I_{ion,n} = G_{m,n}V_n$). The ionic membrane current in the node of Ranvier is not passive. It depends on the dynamics of voltage-gated channels in the nodes, which is formulated as a conductance-based voltage-gated model, such as the Chiu-Ritchie-Rogart-Stagg-Sweeney (CRRSS) model. Detailed information on equations and parameters can be found in Refs. 34–36.

Equation 2 can be extended to include a more realistic internode morphology by considering the periaxonal space (gap between the myelin sheath and axonal membrane). A double cable can include these morphologies, such as the McIntyre-Richardson-Grill (MRG) model,[18,37] in which the nodes of Ranvier's membrane include fast sodium, persistent sodium, slow potassium channels, and leakage conductance.

Both models were implemented to calculate the activation threshold (the lowest stimulation intensity required to propagate an action potential in a given neuron) of a myelinated neuron, which was 22 mm in length, during cortical stimulation of fast-conducting thickly myelinated pyramidal fibres (Betz cell's axon).

A Betz cell's axon diameter measures approximately 5–20 µm as determined in humans and primates.[38,39] The elicitation of an action potential was indicated by the depolarization of the transmembrane potential by 80 mV in at least three consecutive nodes, which is a reasonable criterion for the waveforms in the present study. The amplitude of the stimulation current was modified using a binary search algorithm to find the activation threshold until the error was lower than 10 µA.

The bending of the pyramidal cell axon was included in the model based on prior anatomical information from stained pyramidal cell images[40,41] and previous computational implementations of nerve bending.[23,42,43] Pyramidal neurons start from the grey matter (layers III and IV), cross the grey-white matter interface almost perpendicularly, and descend to form the pyramidal tracts. In our model, for a plane transverse to the motor hand area (Fig. 2a), the trajectories of the neurons inside the grey matter were computed by setting the grey-white matter interface and superficial cortex to different equipotential values, and then applying the Laplace equation between both boundaries. The resulting electric field lines, which are perpendicular to cortical laminae,[44] are used as axons in the grey matter. The trajectories of these axons are then interpolated with control seeds inside the white matter (midline between the two sulci walls) to generate full pyramidal neurons axons by means of a basis-spline function of the fourth order (Figs. 2b and 2c).
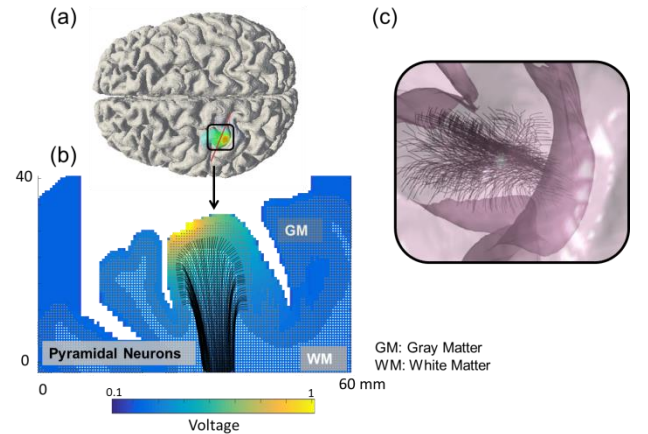


Fig. 2. Pyramidal neurons are embedded in the hand motor area. (a) Brain model and one transversal plane in red (n = 60). (b) Pyramidal neuron trajectories in the white matter of one cross-section. (c) 3D- view of the neurons localization in the brain (n = 2500).

## 2.3. Synaptic Model

MEPs can be evoked via direct excitation of motor area to investigate the integrity of cortical motor pathways during brain surgery. Descending action potentials from the corticospinal tract generate an excitatory postsynaptic potential (EPSP) due to a depolarization current (EPSC) in the postsynaptic membrane. As a result, the EPSP increases the possibility of eliciting an action potential after reaching a threshold. This process is implemented by a synaptic conductance model coupled with a spiking model of the MN.

First, the synaptic conductance was modelled as a dual-exponential function as follows:

$$g_j = g_{\max,j} f \left( e^{-\frac{t}{t_{f,j}}} - e^{-\frac{t}{t_{r,j}}} \right), \qquad (3)$$

where $g_{\max,j}$ is the peak conductance, $t_{r,j}$ and $t_{f,j}$ are the rise and fall time constants that characterize the synapse $j$. The normalization factor $f$ [26] is used to ensure that the amplitude equals $g_{\max,j}$.

The total conductance ($g_{\text{total}}$) is calculated by combining the contribution of each synapse $j$, which is the convolution of all input spike trains ($s_j$) from a corticospinal neuron with the synapse conductance ($g_j$) at the current time $t_x$, as follows:

$$g_{total(t_x)} = \sum_{j=0}^{J} w_j \int_0^{t_x} s_j(\tau) g_j(t_x - \tau) d\tau, \quad (4)$$

where $J$ is the total number of corticospinal neurons synapsing the MN and $s_j$ is described as delta pulses, which represent descending volleys. The parameter $w_j$ is a weighted term, representing synaptic efficacy, which refers to the capacity of a presynaptic input to depolarize the action potential initiation site, thus increasing the probability of cell firing.

The model can be expressed in discrete time $t_n = nT$ employing a Z-transform to improve computation time, as described in detail in reference [45]

$$g_{total}(nT) = C_1 g_{\max,j} \sum_j w_j s_j((n-1)T)$$
$$+ C_2 g_{total}((n-1)T)$$
$$+ C_3 g_{total}((n-2)T). \qquad (5)$$

The term $g_{\max,j} \sum_j w_j s_j((n-1)T)$ can be simplified to $g_{\max} J w s((n-1)T)$ assuming that all synapses have the same weight, $w$, and that there is no delay in the spike trains of different corticospinal neurons, which are

activated simultaneously by cortical stimulation, where C1, C2, and C3 are as follows:

$$C_1 = f \left( e^{-\frac{T}{t_f}} - e^{-\frac{T}{t_r}} \right),$$

$$C_2 = e^{-\frac{T}{t_f}} - e^{-\frac{T}{t_r}} \quad ,$$

$$C_3 = e^{-\frac{T}{t_f}} \cdot e^{-\frac{T}{t_r}} \quad .$$

Second, the total postsynaptic current is modelled as

$$\text{EPSC}(nT) = g_{total}(nT)[E - V_m(nT)], \qquad (6)$$

where $E$ is the synaptic reversal potential and $V_m$ is the postsynaptic membrane potential. The effect of EPSC on activation of the MN is determined using an Izhikevich spiking model [46]

$$\frac{dV_m}{dt} = 0.04 V_m^2 + 5 V_m + 140 - u + EPSPC, \quad (7)$$

$$\frac{du}{dt} = 0.02(0.2 V_m - u). \qquad (8)$$

After the spike reaches 30 mV, the membrane recovery variable $u$ and $V_m$ are reset: $V_m \leftarrow c$ and $u \leftarrow u + d$. Regular spiking pattern was used ($c = -65$ mV, $d = 4$) in the present study.

Finally, the weight of the synapse from a postsynaptic MN depends on the relative timing between presynaptic spike arrivals (spike-timing-dependent plasticity).[47–49] It is a short-term form of homosynaptic facilitation, in which sequential presynaptic pulses produce a larger EPSP, and is thought to be due to residual $Ca^{2+}$ in the presynaptic terminal. A facilitation equation for several consecutive pulses in CMN synapses has been proposed by Muir and Porter.[47,48] Here, we generalized the synaptic weight $w$ (9) to include facilitation, $w_{\text{fac}}$, for $p$ numbers of presynaptic spikes descending from the corticospinal neuron as follows:

$$w_{\text{fac}}(p, w_m) = \begin{cases} w_m \left[ 1 + 0.85 \sum_{p=2}^{p_{\max}} e^{\frac{-(p-1)\Delta t_p}{\tau}} \right] & p > 2 \\ w_m & p = 1 \end{cases} \qquad (9)$$

where $\Delta t_p = t_p - t_{p-1}$ is the time difference between two subsequent pulses, $w_m$ is the synaptic weight of MN without facilitation, and $\tau$ is the time constant equal to 10 ms. The total "gain" is thus given by $g_{\max} J w_{\text{fac}}(p, w_m)$.

The parameters $t_r$ (0.01 ms), $t_f$ (4.9 ms), and $w_m$ (0.002) were obtained by fitting $V_m$ (EPSP) to experimental data (Figs. 5a to 5c) using a non-linear optimization method, while considering $J = 1$, $g_{max} = 5$ nS, and E = 4.6 mV. The parameters $g_{max}$ and E were derived from EPSPs of peripheral Ia pathway activation in the cat.[50] Note that a variation of $g_{max}$ or $J$ values (section 2.4) would be compensated by an inversely proportional variation of $w_m$ during the best-fitting analysis.

## 2.4. *Motor Neuron Pool*

Two techniques for intra-operative cortical electrical stimulation exist, LF and HF stimulations. In HF stimulation, EPSPs overlap and summate with each other (temporal summation) to activate the MN, which is also mediated by facilitation. In contrast, LF stimulation requires a greater activation of corticospinal neurons to trigger the MN by spatial summation.

To investigate the difference between these two techniques, we first computed the necessary number of presynaptic neurons ($j_{LF}$) to trigger a pool of MNs by cortical stimulation at low-frequency (50 Hz, one pulse), as shown in Fig. 6a (red line). The pool was composed of 200 MNs with different synaptic gains, $w_m$. The maximum $w_m$ of the MNs pool was fixed at 0.002 (obtained from experimental EPSPs in section 2.3). The number of presynaptic neurons needed to activate the maximum $w_m$ was $j_{LF} = 116$. Further, we assumed that 10% of the total presynaptic neurons in the model ($j_{LF} = 250$) was the maximum number of connections to the MN pool. Consequently, the minimum $w_m$ of the MNs pool was 0.001. Second, the number of presynaptic neurons ($j_{HF}$) required to activate each MN in the pool during HF stimulation was estimated (grey lines in Fig. 6a). Due to temporal summation, $j_{HF}$ was expected to be lower than $j_{LF}$ for activating each MN in the pool. Finally, we mapped the number of activated presynaptic neurons to stimulation amplitude using the data presented in Fig. 6b. The present study assumed that an MEP was generated when an action potential was elicited in a MN, and that all corticospinal axons innervated the same MN.

## 2.5. *Stimulation Conditions/Parameters*

To demonstrate the effectiveness of the new CMN model, monopolar stimulation was investigated using a monophasic square-wave pulse train (LF and HF), as shown in Fig. 1d. The electrodes were spheres, with a
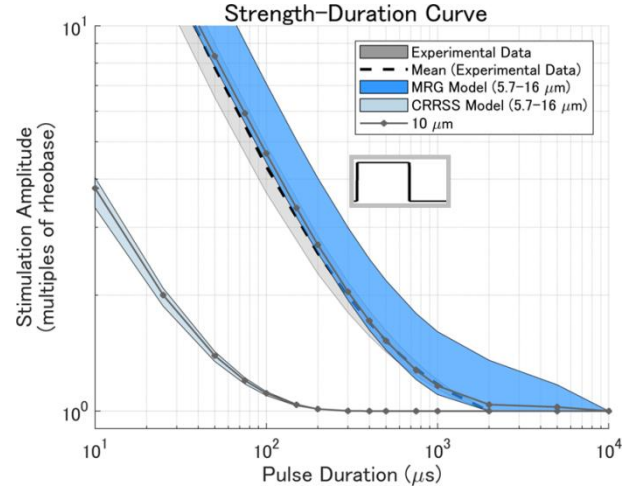


Fig. 3. Strength-duration curves of two myelinated axon models, i.e., the McIntyre-Richardson-Grill (MRG) and Chiu–Ritchie–Rogart–Stagg–Sweeney (CRRSS) models. Experimental data from pyramidal cells were obtained.[51] Monopolar probe and monophasic stimulation were used. For each model, the lower and upper limits correspond to fiber diameter of 16 μm and 5.7 μm, respectively.

diameter of 3 mm (TN210-055 Ojemann-type cortical stimulator probe, Unique Medical Co., LTD, Tokyo). The anode was placed over the motor cortex, while the cathode was placed at the lateral site of the neck. The parameters of the waveform under study were frequency (pulse repetition rate), pulse duration (duration of a single pulse within the pulse train), number of pulses, and intensity (injected current amplitude). To evaluate the pyramidal neuron axon model in subsections 3.1 and 3.2, a monophasic square-wave of a single pulse was used.

## 3. Results

### 3.1. *Strength Duration (CRRSS vs. MRG)*

The simulated strength-duration curves in Fig. 3 were obtained during the cortical stimulation of two axon models (CRRSS and MRG, section 2.2) that were embedded in the volume conductor model of the head below the centre of the stimulating electrode (section 2.1). The computed strength-duration relations were compared to the data obtained from six human subjects[51] to investigate which model was more suitable for cortical stimulation. A square-wave constant current generated corticospinal volleys (D-wave), with amplitudes of 5 μV to 15 μV, via spiral needle electrodes inserted into the scalp. D-waves were

recorded using bipolar electrodes inserted into the epidural space of the spinal cord. The MRG model with diameters between 10 μm and 16 μm were closer to experimental data.

The chronaxie value, which represents the pulse duration required to double the lowest stimulation intensity, was obtained from the strength-duration curve. As seen in Fig. 3, chronaxie values obtained using the MRG model (290.7–617.0 μs) were within the experimental range (257.8–347.4 μs). In contrast, the chronaxie range obtained using CRRSS was between 24.2–28.1 μs. Additionally, microsimulation of pyramidal neurons of the motor cortex of the cats has shown chronaxie values between 100–400 μs.[52]

### 3.2. *Activation Threshold*

The nerve activation threshold is affected by its fiber diameter (axon and myelin) and its initial position in the cortex (cortical depth). We used the same stimulation scenario as in section 3.1. The fiber diameter was between 5.7 μm and 16 μm, and the cortical depth ranged from 2 mm to 4 mm, taking into account the localization of Betz cells in the cortical layer V.[53] The effect of both parameters is presented in Fig. 4, assuming a cerebrospinal fluid thickness of 0.5 mm. Cortical stimulation studies[54] have reported that a pulse duration longer than 0.1 ms requires a minimum threshold of 5 mA to generate an MEP. If one nerve is used to represent this behavior, it is likely that the excitation threshold of a pyramidal neuron (just under the stimulating electrode at 2–4 mm from the cortex) is lower than the threshold required for an MEP response. Under this criterion, a neuron axon model with a diameter of 10 μm that initiates from the grey matter is a good candidate, and has therefore been used in the current study.

### 3.3. *Synaptic Effect*

The temporal/spatial summation and facilitation of EPSPs (6), which were generated by descending action potentials after cortical stimulation of pyramidal neurons was coupled with a motor axon model (7-8), as shown in Fig. 1. The synapse model was validated using intracellular recordings of corticomotoneuronal EPSPs induced by anodal cortical stimulation in monkeys,[47] as shown in Figs. 5a–5c.
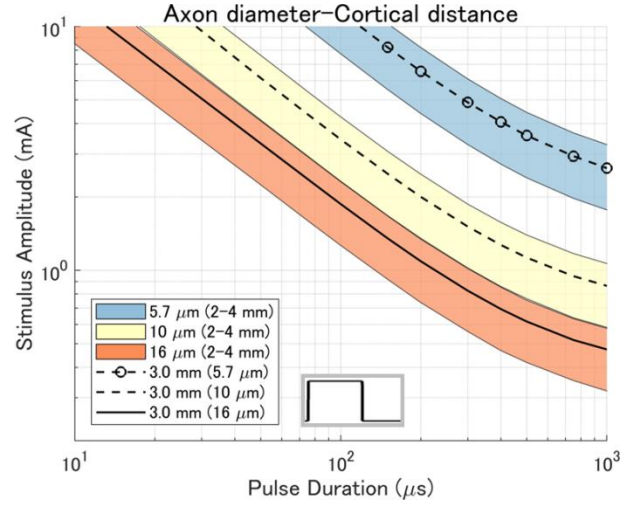


Fig. 4. Excitation thresholds using the McIntyre-Richardson-Grill axon model of a pyramidal neuron embedded in the gyral crown of the hand motor area. Comparison between different distances from the cortical surface to the neuron initial point (2.0–4 mm), and different neuron axon diameters (5.7−16 μm). The pulse of a monophasic current is delivered via monopolar electrodes.

Spike-timing-dependent plasticity (facilitation) was included in (9), as shown in Fig. 5d. Facilitation increased at a higher frequency and strengthened in subsequent pulses. At low frequencies, facilitation became weaker for an initial pulse and continuously decreased with successive pulses. Figs. 5a–5c show a good match between experimental data and a synaptic model, which included a facilitation mechanism. In contrast, the synaptic model lacking facilitation underestimated the generated EPSP.

### 3.4. *Parameter Effect Using the CMN Model*

Figure 6a shows the number of presynaptic neurons that are required to excite each MN in the pool (section 2.4). The stimulus threshold required to activate a specific number of neurons is obtained by the volume conductor model of the head. Figure 6b presents the excitation threshold maps in the motor hand area under the anodic electrode with a pulse duration of 200 μs.

Figure 6c shows the excitation threshold required to activate each MN in the pool (section 2.4) from 50 to 500 Hz at a different number of pulses. The results were rescaled to the range [0, 1] using the maximum threshold required to activate each MN at 50 Hz. LF stimulation (< 100 Hz) required a larger number of pulses than HF stimulation to reduce excitation intensity
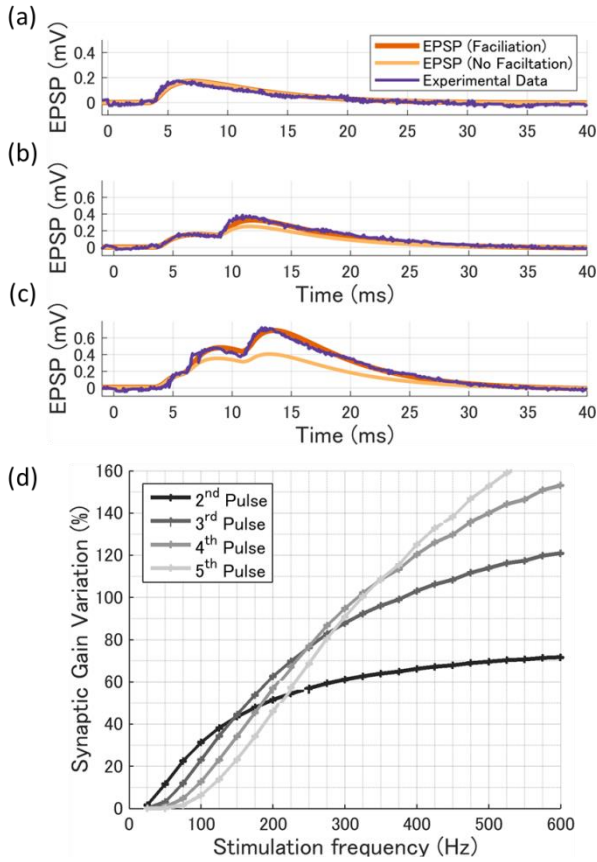
Fig. 5. (a-c) Synapse model verification using intracellular recordings in the corticomotoneuronal synapse[47] for one, two (500 Hz), or three sequential spikes (500 Hz and 200 Hz). Inclusion of the effect of the spike-timing-dependency plasticity (facilitation) improved the results of the model. (d) Spike-timing-dependent plasticity of the motor neuron using a train of pulses delivered at different frequencies in the presynaptic neuron.

to 30%. In contrast, HF stimulation showed greater threshold reduction than LF stimulation using less than 10 pulses. The threshold intensity was reduced by 20% from a train of 5–10 pulses in HF stimulation. Further additional pulses did not lead to significant improvement (4%). Also, the threshold variation was only 4% between 400–500 Hz for a train of 5 pulses, which is a common frequency range in HF stimulation.[1] Variation of cortical stimulation thresholds using a train of 250 pulses or more in a monkey showed a pattern similar to the one found in our results,[55] where a current stimulation of 0.1 ms was applied to the hand motor area using an anodic electrode of 1 mm of diameter. Taniguchi et al.[17] also reported that a small MEP could be recorded at 200 Hz, which was evident between 400–

500 Hz, as our study suggests. After 500 Hz, the CMN tract cannot repetitive respond to each stimulation pulse. The authors also showed that the MEP was perceived initially using a train of two pulses and was evident using 3–5 pulses, which was also indicated by our model.

Figure 6d compares the relationship between two intraoperative stimulation techniques, i.e., the LF and HF stimulations. A large number of pulses were required to reduce the intensity below 100 Hz. Although HF stimulation was applied from 100–200 Hz, its frequency increments did not compensate for the effect of large numbers of pulses in the LF stimulation. For frequencies greater than 200 Hz, the threshold was reduced by using a train of 5–10 pulses.

## 4. Discussion

The assessment of the different stimulation parameters is limited during intraoperative surgery. Extended numerical modelling of CNS electrostimulation was implemented to predict the interaction between electrode configuration/geometry and stimulation waveform parameters. The current study focused on the model implementation and verification to investigate two techniques of intraoperative cortical stimulation, i.e., LF[16] and HF.[17]

### 4.1. *CMN Model*

The proposed CMN model combines the contributions at cortical and synaptic levels to investigate the effect of stimulation parameters in the activation threshold during cortical stimulation. Cortical levels comprise the computation of the electric field generated by cortical electrodes (section 2.1) and its effect on pyramidal neuron activation (section 2.2). Synaptic levels consider the spatial/temporal summation of descending action potentials on motor neuron activation (section 2.3). Most previous studies on brain stimulation modelling focused on the computation of the electric field in the brain.[6,8,14,23,25,43,56–58] These models are pivotal to understanding the location of stimulation hotspots in the brain. However, the effects of the interaction between frequency and pulses delivered to the brain cannot be addressed by those models without considering the integration process at cortical and synaptic levels.

Two conventional neuronal models (i.e., CRRSS[34,35] and MRG[18]) were compared, using experimental strength-duration curves from pyramidal neurons. MRG
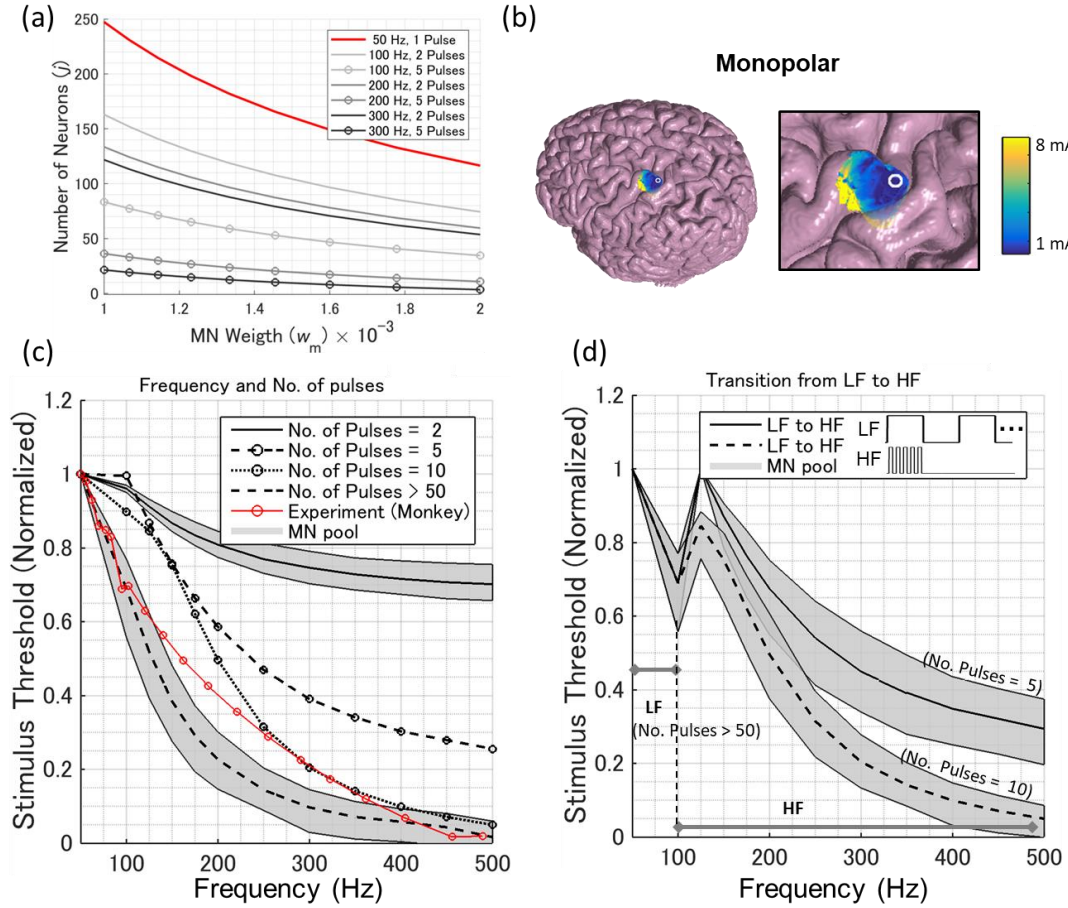
Fig. 6. (a) The number of neurons required to activate each motor neuron (MN) with synapse weight $w_m$. (b) Cortical maps of excitation thresholds using monopolar stimulation for a pulse duration of 200 μs. (c) Excitation thresholds using variable frequencies and numbers of pulses. (d) Transition from low-frequency (LF) and multi-pulse train stimulation (HF) using high and low of pulses, respectively.

was consistent with experimental measurements, while CRRSS showed saturation to the minimum threshold, which was faster than what the experimental data suggested (Fig. 3). A similar result was obtained for transcutaneous electrical stimulation of peripheral nerves.[59] We also noted that the fiber diameter (axon plus myelin) did not lead to any variations in the normalized strength-duration curve. The stimulation intensity required to generate an MEP varied,[60] and depend on the stimulation parameters, the area of stimulation, the tumor location, and MEP monitoring method (needle or surface electrode). Therefore, it is difficult to measure and quantify the spatial distribution or number of pyramidal neurons required to generate an MEP. To have plausible computed stimulation thresholds, we used the minimum excitation current

intensity as a criterion to generate an MEP during intraoperative stimulation.[1]

From the analysis presented in section 3.2, fibers of 10 μm exhibited a threshold, which met this criterion. Further, Firmin et al.,[39] demonstrated that fibers with diameters of 10 μm are most commonly found in the pyramidal tract, which originates from the motor cortex in primates. Here, we only considered a single pulse at the level of the pyramidal axon as multiple pulses do not have any effect on the threshold reduction for a pulse repetition rate lower than 1.5 kHz.[61]

The temporal/spatial summation of CMN EPSPs was modelled and validated with experimental measurements in monkeys, as shown in Fig. 5.[47] The importance of including the spike-timing-dependency plasticity in the synaptic model is also demonstrated in Fig. 5. The resulting EPSP was coupled with a spiking

model of the motor neuron to determine MEP generation.

The results in section 3.4 (Fig. 6c) also show that the proposed CMN model agrees with experimental data, in which a reduction of the stimulation threshold is due to the effect of the stimulating frequency and number of pulses delivered to the motor area.[17,55] Taniguchi et al.[17] demonstrated that an anodal rectangular train of 3–5 pulses, with frequencies between 200–700 Hz, applied to the primary motor cortex, generated MEPs. The temporal summation of frequencies lower than 100 Hz was very small. For frequencies larger than 600 Hz, the refractory period limited repetitive generation of action potentials. This result demonstrated the feasibility and importance of integrating the processes from motor cortex stimulation to MN activation within one neuronal system. In addition, evidence has shown that anodal rectangular pulses delivered at HF stimulation required less intensity, than if delivered at LF stimulation in the primary motor cortex, as shown in Fig. 6d.[62,63] However, the applied technique may have a different performance for other cortical regions. For instance, LF stimulation was more effective in the premotor frontal cortex, supplementary motor cortex,[62] and assessment of speech arrest.[64] LF stimulation techniques (50–60 Hz) may also induce synaptic activity in the cortex by prolonged exposure to stimulation, possibly affecting the thresholds.[65]

## 4.2. CMN Model Simplifications and Limitations

The pyramidal tracts were assumed to be large-diameter, myelinated axons, for a number of reasons. Firstly, motor evoked potentials are induced via direct excitation of Betz's pyramidal cells as they have larger diameters, which facilitate its activation with lower intensity. Secondly, anodal stimulation in the cortical grey matter may initiate neuronal activation at the proximal axonal segments of cortical pyramidal cells (initial segment or segments close to the axon bending), rather than dendrites or soma (direct corticospinal descending volley or D-wave),[21,66] as axonal segments are two to three times more susceptible to polarization than the soma.[67] Thirdly, a simulation model considering the dendrite and soma has shown that these are not significant for large-diameter neuronal fibers, such as Betz cells (supplementary material in reference[14]). Fourthly, the bending of the axon trajectories may influence the results, but its effects are

not substantial because the electrode placed on the gyrus crown preferentially activates straight axons located under the electrode. In contrast, the bending is large in the neurons projecting from the wall, but those neurons are more difficult to activate (since their electric field is weaker and roughly normal to the nerves at the bending). Therefore, no substantial variations were expected from the computed results, particularly for HF stimulation (since fewer pyramidal neurons were required to be activated).

Our assumption did not include experimental verification of the spatial extent of activation and the number/diameter of pyramidal neurons necessary to generate an MEP, which is a limitation of the current study. Statistics of axon thickness has not been reported until now, and thus we applied a single axon thickness in our computation based on experimental measurements. Thus, future experimental measurements are required. Finally, note that the tumor was not included in the realistic head model because it is still uncertain how the trajectories of the pyramidal nerves would change.

We integrated the EPSC model with the Izhikevich model to observe the effect of a train of pulses delivered at different frequencies in the MNs. The Izhikevich model was chosen with a regular spiking pattern. Other spiking patterns, such as chattering (c = -50 mV and d = 2) did not lead to differences in the results (Fig. 6c). The reason is that only the first spike (initial fire), instead of a complex spike pattern, was considered to indicate MN activation. To account for the sum of spiking activities of the pool of MNs, which describes the muscle activity, the neural drive to muscle models[29,68,69] can be adopted in our approach. We have based our assumptions in literature parameters and verified the results with experimental measurements though all the model step.

## 4.3. CMN Activation

Corticospinal neurons, originating from the primary cortex, make direct connections with target MNs, which is important for dexterity and represents a feature unique to certain primate species.[70] However, most neurons in the motor cortex act via interneurons in the spinal cord. In addition, Betz cells only represent 12% of pyramidal cells.[38,71] This study can be extended to include the effects of interneurons, and therefore provide a more detailed representation of MN activation.[28] Finally, direct cortical stimulation was

assumed in craniotomy under general anesthesia in the present study. Thus, D-waves were elicited directly from the axons of a pyramidal neuron,[72] while I-waves were suppressed.[17,73,74] To consider the effects of I-waves[75,76] produced during direct cortical stimulation under awake craniotomy, cortical circuits to pyramidal neurons should be included so that I-waves can also contribute to the temporal summation at the level of the postsynaptic MN. Finally, this approach can be extended to investigate parameters effect during transcranial magnetic stimulation.[77]

## 5. Conclusion

The present study proposes a corticomotoneuronal computational model for intraoperative cortical stimulation. For the first time, the proposed model can investigate the interaction between frequency and number of pulses by integrating cortical stimulation and corticospinal neuron-, synaptic-, and motor neuron-activation into one system. Our results were verified by experimental measurements and provided a computational explanation for the effects of multi-pulse high-frequency and low-frequency stimulation, which could not be addressed by computing only the potential distribution in the brain, as the traditional approach when using volume conductor models.

## Acknowledgements

## 6. References

1. T. Saito, Y. Muragaki, T. Maruyama, M. Tamura, M. Nitta and Y. Okada, Intraoperative functional mapping and monitoring during glioma surgery, *Neurologia Medico-Chirurgica*. (**55**)(1) (2015) 1–13.

2. E. Shiban, S. M. Krieg, B. Haller, N. Buchmann, T. Obermueller, T. Boeckh-Behrens, M. Wostrack, B. Meyer and F. Ringel, Intraoperative subcortical motor evoked potential stimulation: how close is the corticospinal tract?, *Journal of Neurosurgery*. (**123**)(3) (2015) 711–720.

3. S. Krieg, E. Shiban, D. Droese and J. Gempt, Predictive value and safety of intraoperative neurophysiological monitoring with motor evoked potentials in glioma surgery, *Neurosurgery* . (**70**)(5) (2012) 1060–1071.

4. K. Seidel, J. Beck, L. Stieglitz, P. Schucht and A. Raabe, The warning-sign hierarchy between quantitative subcortical motor mapping and continuous motor evoked potential monitoring during resection of supratentorial brain tumors, *Journal of Neurosurgery*. (**118**)(2) (2013) 287–296.

5. C. Fukaya, K. Sumi, T. Otaka and K. Shijo, Corticospinal descending direct wave elicited by subcortical stimulation, *Journal of Clinical*. (**28**)(3) (2011) 297–301.

6. I. Laakso, S. Tanaka, S. Koyama, V. De Santis and A. Hirata, Inter-subject Variability in Electric Fields of Motor Cortical tDCS, *Brain Stimulation*. (**8**)(5) (2015) 906–913.

7. J. Gomez-Tames, J. Gonzalez and W. Yu, Influence of Different Geometric Representations of the Volume Conductor on Nerve Activation during Electrical Stimulation, *Computational and Mathematical Methods in Medicine*. (**2014**) (2014) 1–10.

8. A. Opitz, M. Windhoff, R. M. Heidemann, R. Turner and A. Thielscher, How the brain tissue shapes the electric field induced by transcranial magnetic stimulation, *Neuroimage*. (**58**)(3) (2011) 849–859.

9. S. Mercer, M. Howell and R. Simpson, Simulation training for the Frontline-realistic preparation for Role 1 doctors, *Of the Royal Army Medical Corps*. (**156**)(2) (2010) 87–89.

10. C. A. Bossetti, M. J. Birdno and W. M. Grill, Analysis of the quasi-static approximation for calculating potentials generated by neural stimulation, *Journal of Neural Engineering*. (**5**)(1) (2008) 44–53.

11. J. Gomez-Tames, Y. Fukuhara, S. He, K. Saito, K. Ito and W. Yu, A human-phantom coupling experiment and a dispersive simulation model for investigating the variation of dielectric properties of biological tissues, *Computers in Biology and Medicine*. (**61**) (2015) 144–149.

12. J. Gomez-Tames, J. Gonzalez and W. Yu, A Simulation Study on the Dominance of the Tissues' Conductivity in the Muscle Recruitment, *Journal of Medical Imaging and Health Informatics*. (**3**)(1) (2013) 72–78.

13. J. Gomez-Tames, J. Gonzalez and W. Yu, A simulation study: Effect of the inter-electrode distance, electrode size and shape in Transcutaneous Electrical Stimulation, in *Eng. Med. Biol. Soc.* (Annual International Conference of the IEEE, San Diego, 2012), pp. 3576–3579.

14. L. Manola, J. Holsheimer, P. Veltink and J. R. Buitenweg, Anodal vs cathodal stimulation of motor cortex: A modeling study, *Clinical Neurophysiology*. (**118**)(2) (2007) 464–474.

15. J. Holsheimer, J. Nguyen, J. Lefaucheur and L. Manola, Cathodal, anodal or bifocal stimulation of the motor cortex in the management of chronic pain?, *Acta Neurochirurgica. Supplement*. (**97**)(Pt 2) (2007) 57–66.

16. W. Penfield and E. Boldrey, Somatic motor and sensory representation in the cerebral cortex of man as studied by electrical stimulation, *Brain*. (**60**)(4) (1937) 389–443.

17. M. Taniguchi, C. Cedzich and J. Schramm, Modification of cortical stimulation for motor evoked potentials under general anesthesia: technical description, *Neurosurgery.* (**32**)(2) (1993) 219–26.

18. C. C. McIntyre, A. G. Richardson and W. M. Grill, Modeling the Excitability of Mammalian Nerve Fibers: Influence of Afterpotentials on the Recovery Cycle, *J Neurophysiol.* (**87**)(2) (2002) 995–1006.

19. W. M. Grill Jr, Modeling the effects of electric fields on nerve fibers: influence of tissue electrical properties, *IEEE Trans Biomed Eng.* (**46**)(8) (1999) 918–928.

20. I. Laakso, H. Matsumoto, A. Hirata, Y. Terao, R. Hanajima and Y. Ugawa, Multi-scale simulations predict responses to non-invasive nerve root stimulation, *Journal of Neural Engineering.* (**11**)(5) (2014) 56013.

21. A. Rahman, B. Lafon and M. Bikson, Multilevel computational models for predicting the cellular effects of noninvasive brain stimulation, *Progress in Brain Research.* (**222**) (2015) 25–40.

22. S. Aonuma, J. Gomez-Tames, I. Laakso, A. Hirata, T. Takakura, M. Tamura and Y. Muragaki, A high-resolution computational localization method for transcranial magnetic stimulation mapping, *NeuroImage.* (**172**) (2018) 85–93.

23. H. Seo, D. Kim and S. C. Jun, Effect of Anatomically Realistic Full-Head Model on Activation of Cortical Neurons in Subdural Cortical Stimulation-A Computational Study, *Scientific Reports.* (**6**)(1) (2016) 27353.

24. A. Wongsarnpigoon and W. M. Grill, Computational modeling of epidural cortical stimulation, *Journal of Neural Engineering.* (**5**)(4) (2008) 443–54.

25. R. Tomio, T. Akiyama, T. Horikoshi, T. Ohira and K. Yoshida, Visualization of the electric field evoked by transcranial electric stimulation during a craniotomy using the finite element method, *Journal of Neuroscience Methods.* (**256**) (2015) 157–167.

26. A. Roth and M. van Rossum, *Modeling Synapses* (The MIT Press, 2009), p. 139-159.

27. W. K. Wong, Z. Wang, B. Zhen and S. Leung, Relationship between applicability of current-based synapses and uniformity of firing patterns, *International Journal of Neural Systems.* (**22**)(4) (2012) 1250017.

28. B. Strack, K. M. Jacobs and K. J. Cios, Simulating vertical and horizontal inhibition with short-term dynamics in a multi-column multi-layer model of neocortex, *International Journal of Neural Systems.* (**24**)(5) (2014) 1440002.

29. M. Badoual, Q. Zou, A. P. Davison, M. Rudolph, T. Bal, Y. Frégnac and A. Destexhe, Biophysical and phenomenological models of multiple spike interactions in spike-timing dependent plasticity, *International Journal of Neural Systems.* (**16**)(2) (2006) 79–97.

30. T. W. Dawson and M. A. Stuchly, High-resolution organ dosimetry for human exposure to low-frequency magnetic fields, *IEEE Transactions on Magnetics.* (**34**)(3) (1998) 708–718.

31. I. Laakso and A. Hirata, Fast multigrid-based computation of the induced electric field for transcranial magnetic stimulation, *Physics in Medicine and Biology.* (**57**)(23) (2012) 7753–65.

32. S. Gabriel, R. W. Lau and C. Gabriel, The dielectric properties of biological tissues: III. Parametric models for the dielectric spectrum of tissues, *Physics in Medicine and Biology.* (**41**)(11) (1996) 2271–2293.

33. D. McNeal, Analysis of a model for excitation of myelinated nerve, *IEEE Transactions on Biomedical Engineering.* (**4**) (1976) 329–337.

34. S. Chiu and J. Ritchie, A quantitative description of membrane currents in rabbit myelinated nerve, *The Journal of Physiology.* (**292**)(1) (1979) 149–166.

35. J. D. Sweeney, J. T. Mortimer and D. Durand, Modeling of mammalian myelinated nerve for functional neuromuscular electrostimulation, *IEEE -97th Ann. Conf. Eng. Med. Biol. Soc. Boston.* (**9**) (1987) 1577–1578.

36. F. Rattay and M. Aberham, Modeling axon membranes for functional electrical stimulation, *IEEE Trans Biomed Eng.* (**40**)(12) (1993) 1201–1209.

37. S. M. Danner, U. S. Hofstoetter, J. Ladenbauer, F. Rattay and K. Minassian, Can the Human Lumbar Posterior Columns Be Stimulated by Transcutaneous Spinal Cord Stimulation? A Modeling Study, *Artificial Organs.* (**35**)(3) (2011) 257–262.

38. C. Rivara, C. Sherwood, C. Bouras and P. Hof, Stereologic characterization and spatial distribution patterns of Betz cells in the human primary motor cortex, *The Anatomical Record.* (**270A**)(2) (2003) 137–151.

39. L. Firmin, P. Field, M. A. Maier, A. Kraskov, P. A. Kirkwood, K. Nakajima, R. N. Lemon and M. Glickstein, Axon diameters and conduction velocities in the macaque pyramidal tract, *Journal of Neurophysiology.* (**112**)(6) (2014).

40. K. Amunts and K. Zilles, Architectonic Mapping of the Human Brain beyond Brodmann, *Neuron.* (**88**)(6) (2015) 1086–1107.

41. J. K. Mai and G. Paxinos, *The human nervous system* (Elsevier Academic Press, 2012), p. 1415.

42. B. D. Goodwin and C. R. Butson, Subject-Specific Multiscale Modeling to Investigate Effects of Transcranial Magnetic Stimulation, *Neuromodulation: Technology at the Neural Interface.* (**18**)(8) (2015) 694–704.

43. A. Nummenmaa, J. A. McNab, P. Savadjiev, Y. Okada, M. S. Hämäläinen, R. Wang, L. L. Wald, A. Pascual-Leone, V. J. Wedeen and T. Raij, Targeting of White Matter Tracts with Transcranial Magnetic Stimulation, *Brain Stimulation.* (**7**)(1) (2014) 80–84.

44. S. E. Jones, B. R. Buchbinder and I. Aharon, Three-dimensional mapping of cortical thickness using Laplace's equation, *Human Brain Mapping*. (**11**)(1) (2000) 12–32.

45. J. Köhn and F. Wörgötter, Employing the Z-transform to optimize the calculation of the synaptic conductance of NMDA and other synaptic channels in network simulations, *Neural Computation*. (**10**)(7) (1998) 1639–1651.

46. E. M. Izhikevich, Simple model of spiking neurons, *IEEE Transactions on Neural Networks*. (**14**)(6) (2003) 1569–1572.

47. R. B. Muir and R. Porter, The effect of a preceding stimulus on temporal facilitation at corticomotoneuronal synapses, *The Journal of Physiology*. (**228**)(3) (1973) 749.

48. R. Porter, Early facilitation at corticomotoneuronal synapses, *The Journal of Physiology*. (**207**)(3) (1970) 733–45.

49. N. C. Petersen, J. E. Butler, J. L. Taylor and S. C. Gandevia, Probing the corticospinal link between the motor cortex and motoneurones: some neglected aspects of human motor cortical function, *Acta Physiologica*. (**198**)(4) (2010) 403–416.

50. A. S. Finkel and S. J. Redman, The synaptic current evoked in cat spinal motoneurones by impulses in single group 1a axons, *The Journal of Physiology*. (**342**) (1983) 615–32.

51. D. Burke, K. Bartley, I. J. Woodforth, A. Yakoubi and J. P. Stephen, The effects of a volatile anaesthetic on the excitability of human corticospinal axons, *Brain : A Journal of Neurology*. (2000) 992–1000.

52. E. J. Tehovnik, A. S. Tolias, F. Sultan, W. M. Slocum and N. K. Logothetis, Direct and indirect activation of cortical neurons by electrical microstimulation, *Journal of Neurophysiology*. (**96**)(2) (2006) 512–21.

53. J. DeFelipe, L. Alonso-Nanclares and J. I. Arellano, Microstructure of the neocortex: Comparative aspects, *Journal of Neurocytology*. (**31**)(3–5) (2002) 299–316.

54. K. Kamada, T. Todo, T. Ota, K. Ino, Y. Masutani, F. Takeuchi, K. Kawai and N. Saito, The motor-evoked potential threshold evaluated by tractography and electrical stimulation, *Journal of Neurosurgery*. (**111**)(4) (2009) 785–95.

55. J. C. Lilly, G. M. Austin and W. W. Chambers, Threshold movements produced by excitation of cerebral cortex and efferent fibers with some parametric regions of rectangular current pulses (cats and monkeys), *Journal of Neurophysiology*. (**15**)(4) (1952) 319–41.

56. M. Parazzini, S. Fiocchi, I. Liorni, A. Priori and P. Ravazzani, Computational modeling of transcranial direct current stimulation in the child brain: implications for the treatment of refractory childhood focal epilepsy, *International Journal of Neural Systems*. (**24**)(2) (2014) 1430006.

57. Z. Manoli, M. Parazzini, P. Ravazzani and T. Samaras, The electric field distributions in anatomical head models during transcranial direct current stimulation for post-stroke rehabilitation, *Medical Physics*. (**44**)(1) (2017) 262–271.

58. L. Mai, S. Ueno, T. Thorlin and M. Persson, Calculating the Current Density and Electric Field in Human Head by Multichannel Transcranial Magnetic Stimulation, *IEEE Transactions on Magnetics*. (**45**)(3) (2009) 1662–1665.

59. A. Kuhn, T. Keller, M. Lawrence and M. Morari, A model for transcutaneous current stimulation: simulations and experiments, *Medical & Biological Engineering & Computing*. (**47**)(3) (2009) 279–289.

60. Y. Uno and K. Saito, Structure of cylindrical tissue-equivalent phantom for medical applications, *Electromagnetics in Advanced Applications*. (2010) 406–409.

61. J. P. Reilly, Peripheral nerve stimulation by induced electric currents: Exposure to time-varying magnetic fields, *Medical & Biological Engineering & Computing*. (**27**)(2) (1989) 101–110.

62. T. Kombos, O. Suess, B. C. Kern, T. Funk, T. Hoell, O. Kopetsch and M. Brock, Comparison between monopolar and bipolar electrical stimulation of the motor cortex, *Acta Neurochirurgica*. (**141**)(12) (1999) 1295–301.

63. A. Szelényi, L. Bello, H. Duffau, E. Fava, G. C. Feigl, M. Galanda, G. Neuloh, F. Signorelli and F. Sala, Intraoperative electrical stimulation in awake craniotomy: methodological aspects of current practice, *Neurosurgical Focus*. (**28**)(2) (2010) E7.

64. M. Riva, E. Fava, M. Gallucci, A. Comi, A. Casarotti, T. Alfiero, F. A. Raneri, F. Pessina and L. Bello, Monopolar high-frequency language mapping: can it help in the surgical management of gliomas? A comparative clinical study, *Journal of Neurosurgery*. (**124**)(5) (2016) 1479–89.

65. J. P. Reilly and A. Hirata, Low-frequency electrical dosimetry: research agenda of the IEEE International Committee on Electromagnetic Safety, *Physics in Medicine and Biology*. (**61**)(12) (2016) R138–R149.

66. L. G. Nowak and J. Bullier, Axons, but not cell bodies, are activated by electrical stimulation in cortical gray matter, *Experimental Brain Research*. (**118**)(4) (1998) 489–500.

67. A. Rahman, D. Reato, M. Arlotti, F. Gasca, A. Datta, L. C. Parra and M. Bikson, Cellular effects of acute direct current stimulation: somatic and synaptic terminal effects, *The Journal of Physiology*. (**591**)(10) (2013) 2563–78.

68. D. Farina and F. Negro, Common Synaptic Input to Motor Neurons, Motor Unit Synchronization, and Force Control, *Exercise and Sport Sciences Reviews*. (**43**)(1) (2015) 23–33.

69. R. R. L. Cisi and A. F. Kohn, Simulation system of spinal cord motor nuclei and associated nerves and muscles, in a Web-based architecture, *Journal of Computational Neuroscience*. (**25**)(3) (2008) 520–542.

70. R. N. Lemon, Descending pathways in motor control, *Annual Review of Neuroscience*. (**31**) (2008) 195–218.

71. C. L. Witham, K. M. Fisher, S. A. Edgley and S. N. Baker, Corticospinal Inputs to Primate Motoneurons Innervating the Forelimb from Two Divisions of Primary Motor Cortex and Area 3a, *The Journal of Neuroscience : The Official Journal of the Society for Neuroscience*. (**36**)(9) (2016) 2605–16.

72. Y. Terao and Y. Ugawa, Basic mechanisms of TMS, *Journal of Clinical Neurophysiology : Official Publication of the American Electroencephalographic Society*. (**19**)(4) (2002) 322–43.

73. Y. Katayama, T. Tsubokawa, S. Maejima, T. Hirayama and T. Yamamoto, Corticospinal direct response in humans: identification of the motor cortex during intracranial surgery under general anaesthesia, *Journal of Neurology, Neurosurgery, and Psychiatry*. (**51**)(1) (1988) 50–9.

74. S. G. Boyd, J. C. Rothwell, J. M. Cowan, P. J. Webb, T. Morley, P. Asselman and C. D. Marsden, A method of monitoring function in corticospinal pathways during scoliosis surgery with a note on motor conduction velocities, *Journal of Neurology, Neurosurgery, and Psychiatry*. (**49**)(3) (1986) 251–7.

75. C. V Rusu, M. Murakami, U. Ziemann and J. Triesch, A model of TMS-induced I-waves in motor cortex, *Brain Stimulation*. (**7**)(3)n.d. 401–14.

76. C. C. McIntyre, W. M. Grill, D. L. Sherman and N. V Thakor, Cellular effects of deep brain stimulation: model-based analysis of activation and inhibition, *Journal of Neurophysiology*. (**91**)(4) (2004) 1457–69.

77. J. Gomez-Tames, A. Hamasaka, I. Laakso, A. Hirata and Y. Ugawa, Atlas of optimal coil orientation and position for TMS: A computational study, *Brain Stimulation*. (2018).